Monte Carlo dosimetry for ^{125}I and ^{103}Pd eye plaque brachytherapy

R. M. Thomson,[a] R. E. P. Taylor, and D. W. O. Rogers
Ottawa Carleton Institute of Physics, Carleton University Campus, Ottawa, K1S 5B6 Canada

(Received 21 April 2008; revised 22 September 2008; accepted for publication 22 September 2008; published 13 November 2008)

A Monte Carlo study of dosimetry for eye plaque brachytherapy is performed. BrachyDose, an EGSnrc user code which makes use of Yegin's multi-geometry package, is used to fully model ^{125}I (model 6711) and ^{103}Pd (model 200) brachytherapy seeds and the standardized plaques of the Collaborative Ocular Melanoma Study (COMS). Three-dimensional dose distributions in the eye region are obtained. In general, dose to water is scored; however, the implications of replacing water with eye tissues are explored. The effect of the gold alloy (Modulay) backing is investigated and the dose is found to be sensitive to the elemental composition of the backing. The presence of the silicone polymer (Silastic) seed carrier results in substantial dose decreases relative to water, particularly for ^{103}Pd. For a 20 mm plaque with a Modulay backing and Silastic insert, fully loaded with 24 seeds, the dose decrease relative to water is of the order of 14% for ^{125}I and 20% for ^{103}Pd at a distance of 1 cm from the inner sclera along the plaque's central axis. For the configurations of seeds used in COMS plaques, interseed attenuation is a small effect within the eye region. The introduction of an air interface results in a dose reduction in its vicinity which depends on the plaque's position within the eye and the radionuclide. Introducing bone in the eye's vicinity also causes dose reductions. The dose distributions in the eye for the two different radionuclides are compared and, for the same prescription dose, ^{103}Pd generally offers a lower dose to critical normal structures. BrachyDose is sufficiently fast to allow full Monte Carlo dose calculations for routine clinical treatment planning. © *2008 American Association of Physicists in Medicine*.
[DOI: 10.1118/1.3002412]

Key words: Monte Carlo, dose calculation, eye plaque, EGSnrc, BrachyDose, COMS, I-125, Pd-103, choroidal melanoma

I. INTRODUCTION

Choroidal melanoma is the most common intraocular cancer for adults. In the mid-1980s, the Collaborative Ocular Melanoma Study (COMS) was launched to evaluate therapeutic interventions for this cancer. In the COMS medium tumor trial, patients were entered into a randomized study comparing episcleral ^{125}I plaque therapy with enucleation (removal of the eye).[1] In 2001, the COMS group reported that survival rates for the two treatments were the same,[2] and this was subsequently confirmed in 2006 (Ref. 3) after a longer-term tracking of patients.

Though there are many different plaque models available, the COMS protocol required the use of plaques of a standardized design,[4] consisting of a dome-shaped gold alloy (Modulay) backing with a cylindrical collimating lip. A silicone polymer (Silastic) carrier holds brachytherapy seeds in place at a distance of 1 mm from the concave front of the plaque. Under the COMS protocol,[5] dosimetry essentially followed the recommendations of Task Group 43 of the American Association of Physicists in Medicine (AAPM) Radiation Therapy Committee:[6] Seeds were treated as point sources with source anisotropy and interseed attenuation ignored, the effects of the gold alloy backing on scatter and attenuation were neglected, the Silastic insert was assumed to be water-equivalent, and the shielding effects of the collimating lip were ignored. The dose to water was calculated, overlooking the effects of the eye-air interface, lead-lined eye patch worn by patients, orbital bones, and various eye tissues.

Given the low energy of the photons from the brachytherapy seeds used for eye plaque therapy, the effect of nearby objects with elemental compositions different from water (i.e., plaque backing, insert, air, etc.) is significant. The effect of the backing has been explored in the literature.[7–12] Though a small dose enhancement (relative to water) exists near the backing due to the emission of fluorescence photons by the gold alloy, the plaque's dominant effect is to decrease the backscatter of radiation, resulting in a significant dose reduction in regions further away from the plaque. With the half-value layer of ^{125}I radiation in pure gold of the order of 0.01 mm, there is very little transmission through the 0.5 mm backing. Astrahan *et al.*,[13] Chiu-Tsao *et al.*,[14] and de la Zerda *et al.*[15] have all attempted to account for the collimation of the primary radiation in the plaque backing and lip in treatment planning. To study the effect of the Silastic insert, Chiu-Tsao *et al.*[14] performed Monte Carlo (MC) simulations and thermoluminescent dosimetry (TLD) measurements with one seed at the center of a COMS 20 mm plaque with a water or pure gold backing and Silastic insert. de la Zerda *et al.*[15] subsequently carried out more extensive TLD measurements of dose distributions for a single seed in a COMS 20 mm alloy plaque with a Silastic insert in a solid-water head phantom. Both groups found that the dose at a distance of about 1 cm from the seed was reduced by about

10% relative to that for a seed in homogeneous water.[14,15] Chiu-Tsao *et al.* reported that the effect of the Silastic insert alone was very close to that for the gold and Silastic combination.[14] de la Zerda *et al.* also studied the effect of introducing an eye-air interface and found that, for a single seed at the center of a 20 mm plaque centered on the posterior pole, the dose decreases by more than 10% near the edge of the eye.[15] A recent reanalysis of the COMS medium tumor trial concluded that incorporating factors to account for source anisotropy, the line source approximation, the gold alloy plaque, and the Silastic seed carrier resulted in a consistent reduction in the calculated dose to structures of interest.[16] Astrahan[17] recently updated Plaque Simulator,[13] a TG-43 ophthalmic plaque dose calculation program, using factors from several of the above-mentioned studies[14,15] to incorporate more of the dosimetric effects of the plaque, insert, and air interface.

While the COMS mandated the use of ^{125}I, another gamma-emitting radionuclide, ^{103}Pd, has also been used for eye plaque brachytherapy.[18–21] With an average characteristic x-ray energy of only 20.74 keV,[22] ^{103}Pd potentially offers an advantage over the higher energy photons (average 28.37 keV) of ^{125}I. The shorter range of the lower-energy photons may result in a lower dose to critical normal structures and, hence, improved toxicity-related treatment outcomes. Eye plaque dosimetry for ^{103}Pd has not been extensively explored. The lower energy of the ^{103}Pd photons likely means the dose distribution is more sensitive to the combined effect of the plaque backing and insert than it is for ^{125}I. TLD measurements for a single ^{103}Pd seed in the central slot of a COMS 20 mm plaque suggest a dose reduction of 16% along the plaque's central axis due to the plaque backing and insert relative to the dose for the same seed in pure water.[23] A few years ago, Finger *et al.* proposed a randomized trial comparing eye plaque therapy using ^{125}I, ^{103}Pd, and ^{106}Ru, a beta-emitting source.[21] Critical to any such study is a comprehensive and accurate understanding of dosimetry for each radionuclide.

Recently, the AAPM formed Task Group 129 under the Therapy Physics Committee to review and assess the literature on eye plaque dosimetry, verify and update dosimetry calculations in articles, and recommend consensus dosimetry parameters relevant for eye plaque brachytherapy. While numerous studies related to ^{125}I plaque brachytherapy have been performed, many have been limited to single seed configurations, though configurations of five or more seeds are usually used in treatment. Further, more accurate data for treatment planning systems are needed. Dosimetric studies for ^{103}Pd eye plaque dosimetry are lacking. Given the sensitivity of ocular structures to radiation and the high incidence of late complications related to eye plaque radiotherapy,[24,25] improved dosimetry for eye plaque brachytherapy is an important goal. Accurate dosimetry might improve tumor control while reducing the incidence and severity of complications.[25,26]

In this work, Monte Carlo methods are used to study dosimetry for ^{125}I and ^{103}Pd eye plaque brachytherapy using COMS-style plaques. The Theragenics (Buford, GA) model 200 seed for ^{103}Pd and the GE Healthcare/Oncura model (Arlington Heights, IL) 6711 for ^{125}I are the focus of this study. The effect of the plaque backing on the dose, in particular the sensitivity to the composition of the backing, is investigated. The attenuation due to the Silastic insert and interseed effects are both studied. Working towards the goal of a complete model of the eye, the effects of introducing an air interface or orbital bones and scoring in various eye materials (rather than water) are explored. Three-dimensional dose distributions are computed for various plaque configurations and doses at critical points of interest are compared for ^{125}I and ^{103}Pd seeds.

A few months after this manuscript was submitted for publication, another eye plaque dosimetry study using Monte Carlo methods appeared.[27]

II. MATERIALS AND METHODS

The Monte Carlo simulations are performed using BrachyDose,[28,29] an EGSnrc[30,31] user-code. Though BrachyDose is capable of modeling electron transport, the low energy of the ^{125}I and ^{103}Pd radionuclides means that secondary electrons have a very small range (less than 0.02 mm for 30 keV electrons in water[32]) and, hence, their energy can be considered to be deposited locally. BrachyDose scores the collision kerma per history in voxels using a tracklength estimator, and at the low energies of interest, this is equivalent to the absorbed dose. In these simulations, the photon energy cutoff is set to 1 keV and Rayleigh scattering, bound Compton scattering, photoelectric absorption, and fluorescent emission of characteristic *K* and *L*-shell x rays are all modeled. Photon cross sections from the XCOM (Ref. 33) database are used for all calculations. Mass-energy absorption coefficients are calculated using the EGSnrc user code *g*. The photon spectra quoted in TG-43U1 (Ref. 22) are used to sample initial photon energies and probabilities for ^{125}I and ^{103}Pd. In general, simulations with 10^{10} histories have sufficiently small 1σ statistical uncertainties to see the behaviors of interest, however, for a subset of simulations the number of histories is increased up to 6×10^{10} in order to more clearly illustrate small effects.

In BrachyDose, Yegin's multi-geometry package[34] is used to fully model brachytherapy sources and eye plaques. Many seed models, including those used in this study, were previously benchmarked via calculations of the TG-43 dosimetry parameters (dose rate constants, radial dose functions, and anisotropy data).[35,36] Detailed dosimetry parameters for the ^{103}Pd (Theragenics model 200) and ^{125}I (GE Healthcare/Oncura model 6711) seed models appear in the Carleton Laboratory for Radiotherapy Physics TG-43 Parameter Database, a publicly accessible web site.[37] Results for both seed models were shown to be in good agreement with the data of other authors.[35–37] Though these two seeds are the focus of this study, all other seeds can be modeled.[36]

COMS standard eye plaques[4] with diameters ranging from 10 to 22 mm (in 2 mm increments) are modeled. Note that the 10 and 22 mm plaque sizes were only made available relatively recently.[38] The plaque backing is a segment of

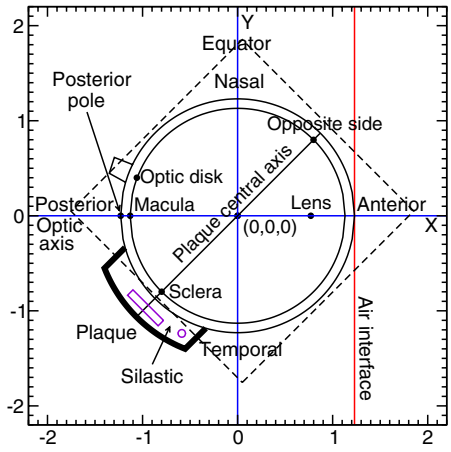

FIG. 1. Points of interest for eye plaque dosimetry, given in the center of eye reference frame (scale in centimeters) for a right eye. The eye is idealized as a sphere of radius 1.23 cm. The (planar) air interface, which is transverse to the optic axis, is shown. The dashed line indicates the extent of the scoring grid, described in Sec. II. While a 12 mm plaque positioned between the posterior pole and equator is shown here, plaques in other positions, e.g., centered on the posterior pole and on the equator nasal and temporal to the eyeball, are also simulated.

a spherical shell which is 0.5 mm thick with a 15.05 mm outer radius of curvature, terminating in a collimating cylindrical segment, or lip, 2.7 mm long[38]—see Fig. 1. The plaque size is specified as the inner diameter of this cylindrical segment (which is also 0.5 mm thick). The seed carrier insert fits snugly into the concave side of the alloy backing and has an inner radius of curvature of 12.3 mm so that plaques fit an eye modeled as a sphere of diameter 24.6 mm. Plaques are constructed of the gold alloy Modulay, which is 77% gold, 14% silver, 8% copper, and 1% palladium by weight.[11] Modulay, with a density of 15.8 g/cm^3 (obtained from http://www.jelenko.com/ENGLISH/alloy_spec/MODULAY-BOOK.pdf, accessed 28 August, 2008), is less dense than pure gold (19.3 g/cm^3). The seed carrier insert is made of Silastic, which is 6.3% hydrogen, 24.9% carbon, 28.9% oxygen, 39.9% silicon, and 0.005% platinum by weight and has a density of 1.12 g/cm^3.[14] The seeds are positioned in concentric rings about the plaque's central axis and are centered on a sphere of radius 13.7 mm. The seed slot positions were provided by TG-129 of the AAPM in 2007 (private communication, S. Chiu-Tsao, 2007), and are available at http://www.physics.carleton.ca/clrp/eye_plaque.

In most simulations, the eye plaque is modeled at the center of a $30\times30\times30$ cm^3 water phantom of mass density 0.998 g/cm^3. However, in a subset of simulations, air or orbital bone is introduced or the water is replaced with various eye materials to scope the effects of these elements of a human eye model. To study the effect of air at the edge of the eye, a portion of the water phantom is replaced with air. As illustrated in Fig. 1, the planar water-air interface is introduced at a distance of 1.23 cm from the center of the (imaginary) eye. A lead eye patch, sometimes worn by patients during ophthalmic treatment, is modeled as a 1 mm thick lead sheet 5 mm away from the eye-air interface. Orbital bones are modeled with a cylinder constructed of skull bone of length 2.46 cm and inner (outer) diameter 3.01 cm (4.01 cm), centered on the eye, with the cylinder openings at the front and back of the (imaginary) eye in the water phantom. With these dimensions, the bone cylinder is just outside the plaque. Some simulations were repeated with the inner (outer) cylinder diameter decreased to 2.46 cm (3.46 cm), to be in contact with the eye itself. The bone composition and density are from ICRU Report 46,[39] and are quoted in Table I. Simulations in which water is replaced with either homogenized eye (a protein-water mixture simulating the composition of the eye (Ref. 40)) or eye lens (Ref. 39)—see Table I—are also performed.

Following the COMS protocol, the origin of the plaque coordinate system is taken to be 1 mm away from the inner surface of the Silastic insert at the center of the plaque, coinciding with the inner sclera. The plaque's central axis defines the z-direction; the x and y coordinates span the directions transverse to this axis. The use of both $0.1\times0.1\times0.1$ mm^3 and $0.5\times0.5\times0.5$ mm^3 voxels was investigated and it was found that the dose distribution could be accurately scored in the region of interest with the larger voxel size. In general, the dose is scored in an array of $0.5\times0.5\times0.5$ mm^3 voxels, with the first voxel centered on $z=-0.5$ mm, and extending out to $z=2.45$ cm—see Fig. 1. In the x and y directions the grid extends from −1.25 to 1.25 cm.

A number of aspects of eye plaque dosimetry are investigated and, in order to connect with TG-43 type calculations, the results are often compared to those from simulations with the same seed configurations in water. The effect of the plaque backing alone is studied by performing simulations with one ^{125}I or ^{103}Pd seed in the central slot of a 12 or 20 mm plaque, with the Silastic insert replaced with water and the backing constructed of pure gold or the gold alloy Modulay. In the coordinate system defined above, the center of this slot is (0,0,−0.24) cm and, on the central axis,

TABLE I. Composition and densities of certain eye tissues and bone used in simulations, taken from ICRU Report 46 (Ref. 39) and ICRP Report 23 (as quoted in Ref. 40).

Tissue/material	Percent by weight elemental composition										Density ($g\,cm^{-3}$)
	H	C	N	O	Na	Mg	P	S	Cl	Ca	
Lens	9.6	19.5	5.7	64.6	0.1	—	0.1	0.3	0.1	—	1.07
Homogenized eye	10.7	3.8	1.2	84.3	—	—	—	—	—	—	1.03
Skull bone	5.0	21.2	4.0	43.5	0.1	0.2	8.1	0.3	—	17.6	1.60

the plaque backing extends from $z=-0.375$ cm to $z=-0.325$ cm. Simulations with one seed at the center of a Silastic insert with no backing are performed to ascertain the effect of the insert alone. For these single seed simulations, it is assumed that all other slots are filled with the insert material. Modulay or pure gold backings are then simulated with a Silastic insert to study the combined effect of the backing and insert on the dose distribution.

Interseed attenuation is studied via simulations of fully loaded 12, 16, and 20 mm plaques (containing 8, 13, and 24 ^{125}I or ^{103}Pd seeds, respectively) in which the plaque and insert are constructed of water or of Modulay and Silastic. Full simulations, which model the interactions of photons with any seed, are compared to simulations with no interseed effects, in which only one seed is "active" at a time: While the transport of photons from the active seed is being simulated, the other seeds are replaced with the insert material.

Having accounted for the effect of the backing and insert, and interseed attenuation, simulations of multiple seeds in the COMS plaques (Modulay backing, Silastic insert) are performed. Three-dimensional dose distributions for each plaque size (scored in water) are available at a publicly accessible web page (http://www.physics.carleton.ca/clrp/eye_plaque). The results of these simulations are compared to simulations of the same configuration of seeds in water (i.e., with the plaque backing and insert replaced with water) with no interseed effects, as these are not included in calculations performed according to the TG-43 protocol.

An air interface is present in several simulations in which the plaque is centered (a) on the posterior pole; (b) on the equator nasal and temporal to the eyeball; (c) midway between the equator and posterior pole as shown in Fig. 1; and (d) on the equator above the eyeball. The dose distributions from these simulations are compared to those in which there is no air interface.

Simulations with the bone cylinder were performed with the plaque centered on the posterior pole for both cylinder diameters, while only the larger diameter was used for the plaque centered on the equator temporal to the eyeball. The dose distributions for these simulations were compared to those in which no bone is present.

The dose distributions for different plaque configurations, sizes, and the two radionuclides are compared via depth-dose curves and by tabulating the dose at the points of interest within the (right) eye noted in Fig. 1. It is important to distinguish the eye reference frame (X,Y,Z), from the plaque reference frame (x,y,z) which was discussed above: The eye coordinate frame (X,Y,Z) has its origin at the eye center and the axis directions are as shown in Fig. 5(a) of the paper by Kepka *et al.*[41] The positions of the points indicated in Fig. 1 are based on the locations indicated by Astrahan[17] and Kepka *et al.*[41] The dose at the sclera is quoted at $(x,y,z)=(0,0,0)$ in the plaque reference frame, i.e., 1 mm inset from the Silastic insert on the plaque's central axis. For this study, $z=0.5$ cm on the plaque's central axis is taken as the tumor apex and dose prescription point. The opposite side of the eye from the plaque (and tumor) corresponds to $z=2.26$ cm on the plaque's central axis. The macular dose is calculated at a point inset 1 mm from the external surface of the eye on the optic axis in the eye's posterior. The optic disk center is taken to be 0.4 cm medial to the optic axis and 1.06 cm posterior to the Y-axis, corresponding to $(-1.06,0.4,0)$ cm in the eye reference frame. The center of the lens is 0.77 cm along the optic axis anterior to the center of the eye, i.e. $(0.77,0,0)$ cm in the eye reference frame. If a point of interest does not correspond with the center of a voxel, the dose is determined by interpolation of the dose values from neighboring voxels.

For a real eye, the relative position of the plaque and the positions of critical structures are only known approximately. Uncertainties on the dose to the structures of interest, depending on the local dose gradient, result. Further, the doses at points of interest off the plaque's central axis (macula, optic disk, and center of lens) depend on the exact positions of seeds in the plaque and vary by up to 3% depending on seed carrier orientation. In this article, the purpose of reporting the dose at these points is to enable comparisons with results for different configurations or from Plaque Simulator,[17] rather than provide the absolute dose at these points. Thus, positional uncertainties are not the primary concern here. The three-dimensional dose distributions on the web page permit the determination of the dose at any location in the eye region.

For the comparison of the doses at points of interest in the eye, the total dose for a treatment is reported and is calculated as follows: The MC simulations provide the dose in a voxel per history. The dose rate is calculated by dividing this number by the air kerma strength per history for the relevant seed type and by multiplying by the number of seeds and the air kerma strength per seed. The air kerma strength per seed is chosen in order to obtain a prescription dose of 85 Gy at the tumor apex in 100 h for ^{125}I and 168 h for ^{103}Pd, where the treatment times were chosen to coincide with those used by TG-129 (S. Chiu-Tsao, private communication, 2007). The total dose delivered during a treatment is then determined by integrating over the treatment time, taking into account the exponential decay of the source.

While results are quoted with statistical uncertainties, there are a number of other causes of uncertainty. As mentioned above, the effect of scoring in different voxel sizes was explored and a detailed discussion of voxel size effects appears in the work of Taylor *et al.*[35] Uncertainties in cross-section data and seed geometry were not investigated; however, these are discussed in detail in TG-43U1.[22] In the vicinity of the seed, uncertainties due to seed geometry and cross-section data are each roughly 2%, while the uncertainty on the source energy spectrum is 0.1%. In the eye plaque model, the six suture eyelets at 30° to each other along the edge of the collimating lip are not modeled. Given the small size and position of the eyelets, it is likely that they have a very small dosimetric effect, especially since the dose is quite small in their vicinity. In simulations, seeds are assumed to be completely surrounded by the insert material. In reality, small air gaps might exist about each seed; however,

TABLE II. Timing for simulations of a fully loaded 16 mm Modulay/Silastic plaque performed on a single 3.0 GHz Woodcrest core, scoring in either $(0.05\ \text{cm})^3$ or $(0.1\ \text{cm})^3$ voxels in water. The times to achieve 2% statistical uncertainty on the dose at either (i) the tumor apex (prescription point, D_p) or (ii) the point on the plaque's central axis where the dose is half the prescription dose ($D=0.5\ D_p$) are given. The statistical uncertainty on the dose at the point at the opposite side of the eye from the plaque (δD) is given as a percentage of the local dose (D_{local}) and of the prescription dose (D_p).

Seed type	Scenario: Required uncertainty	$(0.05\ \text{cm})^3$ voxels			$(0.1\ \text{cm})^3$ voxels		
		Time (min)	δD		Time (min)	δD	
			% of D_{local}	% of D_p		% of D_{local}	% of D_p
^{125}I	2% on D_p	3.0	7.4	0.52	0.57	7.5	0.54
	2% on $D=0.5\ D_p$	5.6	5.3	0.37	1.1	5.1	0.41
^{103}Pd	2% on D_p	2.5	9.8	0.42	0.51	9.0	0.45
	2% on $D=0.5\ D_p$	4.9	7.0	0.28	0.99	6.5	0.32

these would likely have a very small effect. Exact material compositions may differ slightly from those used in this study, and the effects of these variations are difficult to assess in general. As mentioned above, dose sensitivity to the plaque backing material is investigated by performing simulations with pure gold and Modulay backings and by varying the Modulay density. It is not expected that small variations in the composition of the Silastic would significantly affect results. Of course, the elemental compositions and densities of eye materials vary across the population: compositions recommended by the ICRU (Ref. 39) and ICRP (quoted in Ref. 40) are used for the calculations described in Sec. III D. A full investigation of the effects of variations in the density and composition of eye materials is left to a future study which incorporates a full model of the human eye. As discussed above, the uncertainties in the coordinates of points of interest and the plaque position result in uncertainties on the dose dependent on the local dose gradient. Given the small statistical uncertainties on the results presented in this article and the fact that uncertainties in the seed geometry and cross-section data alone are each roughly 2%, uncertainties from other causes are greater than the statistical uncertainties.

The CPU time for a simulation varies slightly with plaque material and position and also with the number and type of seeds. With no variance reduction techniques, a simulation with 10^{10} histories and the grid of $(0.05\ \text{cm})^3$ voxels described above typically takes about 40 h on a single 3.0 GHz Woodcrest core, resulting in a statistical uncertainty of roughly 0.1% on the dose at the prescription point and less than 0.5% on the dose at the points of interest indicated in Fig. 1, with the highest percent uncertainty among these points typically occurring at the point at the opposite side of the eye from the plaque. Note, however, that this point also typically has the lowest dose among the points of interest, with the dose being less than 10% of the prescription dose.

For clinical applications, the calculation time would be substantially less than 40 h because such small statistical uncertainties are not needed. Further, preliminary investigations suggest that scoring in $(0.1\ \text{cm})^3$ voxels should be sufficiently accurate to describe dose distributions in the eye. Scenarios requiring a 2% statistical uncertainty on the dose (i) at the tumor apex (the prescription point), or (ii) at the point on the central axis where the dose drops to half the dose at the tumor apex, were both investigated, for the array of $(0.05\ \text{cm})^3$ voxels described above and also for an array of $(0.1\ \text{cm})^3$ voxels spanning the same region. In order to increase the efficiency of simulations, a particle recycling feature was used in which the first seed in the simulation acts as a particle (photon) generator: Photons initiated in this seed are tracked until they are absorbed in the seed or escape from it. If a photon escapes, it is reinitiated at each seed location after a rotation through a random angle about the seed axis. Correlations between recycled photons from the same primary history are taken into account via history by history statistics.[42] The efficiency gains achieved via particle recycling depend on the voxel size and seed geometry. For seeds in a 16 mm plaque, this recycling feature decreases simulation times by about 40% for ^{125}I and 55% for ^{103}Pd, corresponding to efficiency gains of more than 60% and 100% for ^{125}I and ^{103}Pd, respectively.

The times for each scenario are given in Table II for a 16 mm Modulay/Silastic plaque filled with ^{125}I or ^{103}Pd seeds. The uncertainty at the opposite side of the eye to the plaque (which has the largest uncertainty among the points of interest indicated in Fig. 1), is quoted as a percentage of the local dose, D_{local}, and of the prescription dose, D_p. For scenario (i) (2% uncertainty at the tumor apex) and ^{125}I (^{103}Pd) seeds, the simulation takes 3.0 (2.5) min in $(0.05\ \text{cm})^3$ voxels and 0.57 (0.51) min in $(0.1\ \text{cm})^3$ voxels. The uncertainty on the dose at the opposite side of the eye is 7.4% (9.8%) of the local dose, which amounts to roughly 0.52% (0.42%) of the prescription dose. For the more stringent requirement (ii) (2% uncertainty at 50% of the prescription dose), the calculation times roughly double and the statistical uncertainties at all points of interest are reduced by a factor of about $\sqrt{2} \simeq 1.4$. Note that the statistical uncertainties are nearly the same at the point at the opposite side of the eye for either voxel size, and this is also true at the other critical points of interest in the eye. This suggests that the relative uncertainties through space are independent of the

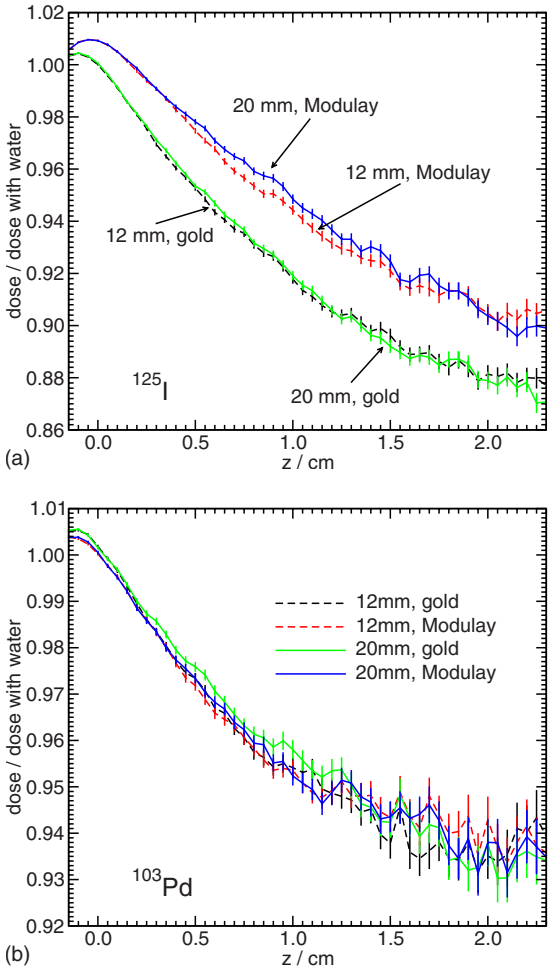

FIG. 2. Ratio of the doses along the plaque's central axis for a single seed at the center of a 12 or 20 mm plaque with a Modulay or gold backing and water insert to the doses with water (no plaque) for (a) ^{125}I and (b) ^{103}Pd.

voxel size, as would be expected in the absence of voxel size effects, and supports the use of $(0.1\ \text{cm})^3$ voxels for clinical treatment planning.

III. RESULTS AND DISCUSSION

III.A. Effect of the plaque backing

The effect of the plaque backing alone is shown in Fig. 2, which provides central axis depth-dose curves for one ^{125}I (a) or ^{103}Pd (b) seed in the central slot of a Modulay or pure gold plaque with water replacing the Silastic insert. The doses for the various configurations are quoted relative to the doses for the same seed in water (no plaque present). For either seed type, while a small dose enhancement is evident near the seed and plaque (small z), the dominant effect is a significant dose decrease which begins a few millimeters away from the seed and increases with z. This dose reduction is due to the high-Z materials of the backing which cause enhanced photoelectric absorption and decreased Compton scatter relative to water. The dose enhancement near the seed and plaque is due to fluorescence photons emitted by atoms in the plaque backing as they relax to a ground state following excitation by photons from the brachytherapy sources. These results are qualitatively in accord with the results of earlier studies on the effect of a high-Z backing.[7–12]

The dose is sensitive to the backing's composition. Both ^{125}I and ^{103}Pd photons excite the L-shell in gold (~14 keV) and K-shell in copper (~9 keV); however, few ^{103}Pd photons can excite the K-shell in silver (~25 keV), which is excited by ^{125}I photons of average energy. The excitation of these shells results in the emission of fluorescence photons with energies just below these thresholds. Clearly, the spectrum of fluorescent photons depends on the energy of photons from the brachytherapy seeds and the backing's composition. Relative to pure gold, the presence of copper and silver in Modulay modifies the spectrum of fluorescent photons and, hence, the dose distribution. Copper acts to decrease the dose because of the lower average energy of the fluorescence photons and, hence, their shorter range. Fewer of these photons escape the backing and those that do escape to the water do not travel far before being absorbed. This results in a slightly lower dose with the Modulay plaque relative to pure gold for ^{103}Pd, as illustrated in Fig. 2(b). The excitation of the K-shell in silver by ^{125}I photons means that the dose is higher with Modulay relative to pure gold, as shown in Fig. 2(a). These observations also explain why the dose enhancement near the plaque is larger for ^{125}I than it is for ^{103}Pd: The higher average energy of ^{125}I photons means that more fluorescence photons and fluorescence photons of higher average energy are emitted from the backing for the ^{125}I source than for ^{103}Pd, resulting in a dose enhancement close to the plaque of the order of 1% for ^{125}I versus 0.5% for ^{103}Pd.

For both ^{125}I and ^{103}Pd with the Modulay backing, the dose decrease at $z=1$ cm is of the order of 5%: a little greater for ^{125}I and a little smaller for ^{103}Pd, both depending very slightly on the plaque size. At $z\simeq 2.3$ cm, i.e., across the eye, the dose decrease due to the Modulay backing is about 10% for ^{125}I and less than 7% for ^{103}Pd. This difference is due to the relative importance of the photoelectric effect and Compton scatter for the ^{125}I and ^{103}Pd photons and the fact that the main effect of the plaque backing is to decrease Compton scatter relative to water. For either pure gold or Modulay, the majority of interactions for ^{125}I and ^{103}Pd photons is photoelectric, with less than 5% of interactions occurring via Compton scatter. For ^{125}I photons (with a mean energy of 28 keV), Compton scatter accounts for 47% of interactions in water while for ^{103}Pd photons (21 keV), only 27% of interactions occur via Compton scatter. Hence, the introduction of the plaque backing is more significant for ^{125}I than for ^{103}Pd.

Chiu-Tsao *et al.*[14] reported a dose decrease of about 10% at $z\simeq 0.76$ cm based on their Monte Carlo simulations of an ^{125}I (model 6711) seed with a 20 mm pure gold backing. The results for the pure gold backing in Fig. 2(a) suggest that the drop-off at this distance is about 7%. Note that the full simulation, taking into account the atomic composition of the Modulay, indicates that this decrease is only 4%.

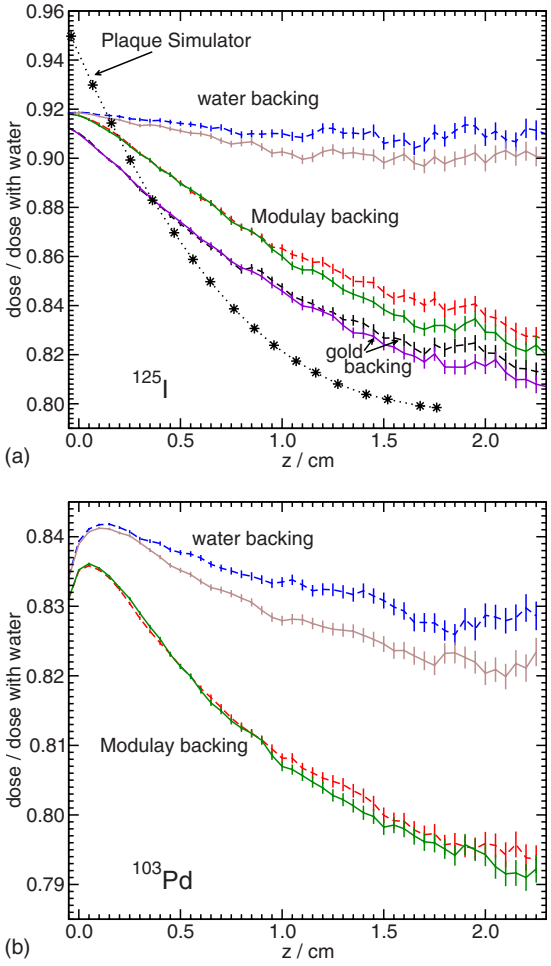

FIG. 3. Ratio of the doses along the plaque's central axis for a single seed in a Silastic insert (backings as indicated) at the center of a 12 (dashed lines) or 20 mm (solid lines) plaque to the doses for the same seed in water (no backing or insert) for (a) ^{125}I and (b) ^{103}Pd.

The sensitivity of the results to the density of Modulay is investigated by performing simulations with the Modulay backing density changed from 15.8 to 14 and 17 g/cm^3. No statistically significant difference is observed.

III.B. Effect of the Silastic insert

The central axis doses for a single seed at the center of a Silastic insert with a water, pure gold, or Modulay backing are reported relative to the doses for the same seed in water in Fig. 3. Silastic, with an effective atomic number of 10.7,[17] is a significantly more attenuating medium than water ($Z_{\text{eff}} \sim 7.4$), and hence its presence results in a significant decrease in dose, even if the backing is replaced with water. This effect is more important for the lower energy photons of ^{103}Pd than it is for ^{125}I, as the former have a significantly shorter mean-free path in Silastic and are more severely attenuated. On the plaque's central axis at $z \simeq 1$ cm, the presence of the Silastic insert alone results in a dose decrease of about 9% for ^{125}I, compared to nearly 17% for ^{103}Pd. For $z < 1.2$ cm, the results for the ^{125}I seed in the 20 cm Silastic insert (water backing) are roughly in agreement with the (noisy) data from the Monte Carlo simulations of Chiu-Tsao *et al.*,[14] however, further away from the plaque their data suggests a dose reduction of close to 20% while Fig. 3(a) shows a 10% decrease. Figures 3(a) and 3(b) indicate that the dose decrease relative to water is somewhat sensitive to the size of the Silastic insert: more attenuation takes place in a larger insert, which leads to some decrease in the scattered dose. For ^{125}I, the decrease is of the order of 1% more for the 20 mm size than for 12 mm, while for ^{103}Pd this decrease is smaller because there is less scatter for low-energy photons.

The shape of the curves for ^{125}I and ^{103}Pd at small z in Fig. 3 are different, with the curves for ^{103}Pd increasing slightly with z before decreasing slowly. This artifact is due to the source geometry for this particular brachytherapy seed:[35,36] the model 200 ^{103}Pd pellets contain two radioactive sources separated by a lead marker. With no radioactivity at the center, photons must travel through more Silastic to reach areas very near the insert on the central axis than to reach areas at slightly larger z. Hence, on the central axis there is more attenuation near the seed than slightly further out, resulting in the increasing dose ratio for small z. This behavior is not evident for the model 6711 ^{125}I seeds, which have a single cylindrical rod as the radioactive source.

The addition of the plaque backing to the Silastic insert results in a further dose decrease, as illustrated in Figs. 3(a) and 3(b). For a single seed in a 12 or 20 mm plaque, the total decrease relative to water at $z=1$ cm on the central axis is almost 14% for ^{125}I and 20% for ^{103}Pd. Note that the combined effect of the insert and plaque is not the product of the effects of the insert and plaque separately, as fluorescent x rays originating in the plaque must now pass through the Silastic insert, and a significant fraction of these photons will be absorbed in the insert. The results for the pure gold backing and Silastic insert with the ^{103}Pd seed are omitted from Fig. 3(b) as they are nearly identical to those for the Modulay backing. For ^{125}I, the sensitivity of the dose to the composition of the backing is still clearly seen with the doses for the Modulay backing enhanced by up to 2% relative to pure gold. As discussed above, the excitation of the *K*-shell in silver followed by the emission of fluorescence photons is responsible for this enhancement.

The results for the combination of backing and insert for the ^{125}I seed in Fig. 3(a) show roughly the same trend as those from the Monte Carlo simulations of a single ^{125}I seed at the center of a Silastic insert and pure gold backing of Chiu-Tsao *et al.*[14] The best-fit line to their data, used in Plaque Simulator,[17] is shown in the figure. It overestimates the dose near the seed and underestimates it further out. Contrary to what is seen in Fig. 3(a), Chiu-Tsao *et al.*[14] concluded that the effect of the Silastic insert alone is nearly the same as that for the Silastic and gold combination. Their conclusion was drawn from a combination of TLD measurements and MC simulations and, in both cases, their data were quite noisy.

Chiu-Tsao *et al.* reported a dose decrease of 16%, relative to water, along the central axis of a COMS 20 mm plaque (backing and insert) containing a single ^{103}Pd seed.[23] The

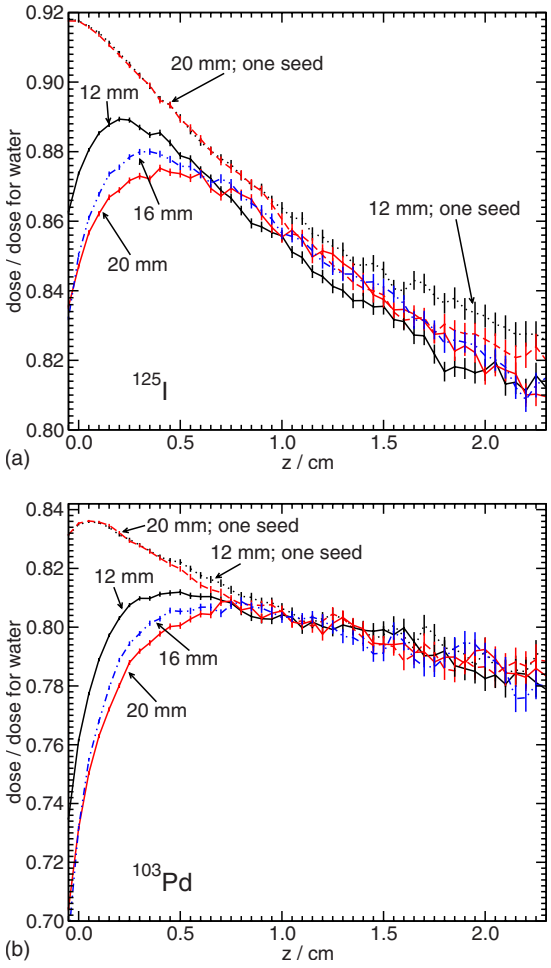

FIG. 4. Comparison of single seed and multiseed results along the plaque's central axis: Ratio of the doses for seeds in a Modulay/Silastic plaque to the doses for the same seeds in water (no plaque) with no interseed effects for different plaque sizes and (a) ^{125}I and (b) ^{103}Pd seeds. Unless otherwise noted, the results are for multiseed simulations.

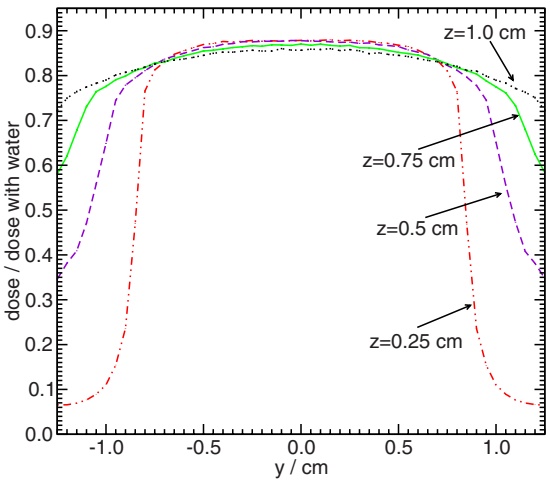

FIG. 5. Effect of collimation due to the plaque: Ratio of the doses for a 16 mm Modulay/Silastic plaque with ^{125}I seeds to the doses for the same seed configuration in water (no plaque, no interseed effects) vs. transverse position y at $x=0$ and for various depths z.

results in Fig. 3 suggest that the dose decrease is 16% to 17% near the seed and becomes 21% at the opposite side of the eye.

III.C. Multiseed configurations and interseed effects

Interseed effects are investigated by comparing the ratios of doses with interseed effects to those without interseed effects for fully loaded 12, 16, and 20 mm plaques. For both ^{125}I and ^{103}Pd seeds in a 20 mm plaque, the effect is of the order of 1% or 2% for seeds in water (no insert or backing) and is much less pronounced, at less than 0.5%, for the Modulay and Silastic combination. The ratio of doses is nearly constant, decreasing slightly, going along the plaque's central axis. The magnitude of interseed effects decreases as plaque size decreases, simply because there are fewer seeds present to attenuate photons from other seeds. Interseed attenuation in the region of interest is much smaller than for other types of brachytherapy, e.g., prostate implants[43] where interseed attenuation is substantial at positions in line with multiple seeds because shadowing is important. The presence of the collimating lip on the plaque means that these positions are not relevant for eye plaques.

The difference in dose distributions for simulations with and without interseed effects suggests that, in order to place this work in the context of calculations performed according to the TG-43 protocol,[6] results should be quoted relative to those for the same configurations of seeds in water (no backing or insert) with no interseed effects. Hence, the results presented in the following for multiseed configurations in water only are from simulations with no interseed effects.

A comparison of the effect of the plaque and backing for single and multiple seed simulations is shown in Fig. 4. Results for single seed simulations are shown for the 12 and 20 mm plaque sizes and not the 16 mm plaque, as the latter does not have a central slot. The effect of the Modulay and Silastic relative to water depends on the number and configuration of seeds present. For small z, the dose ratios for the multiseed configurations are significantly smaller than those for single seeds. This is because photons from seeds at off-axis locations must travel through more Silastic than those from the central seed in order to reach the small z scoring region, resulting in substantial attenuation. This effect increases with plaque size as photons originating from seeds at larger radii (in the larger plaques) are more severely attenuated. At larger z, the dose ratios for single and multiseed configurations are closer: For the 12, 16, and 20 mm fully loaded plaques, the dose decrease at $z=1$ cm on the central axis is 14% for ^{125}I and 20% for ^{103}Pd, roughly the same as the decrease for the 12 and 20 mm plaques with one seed in the central slot (discussed in Sec. III B).

The presence of the plaque results in significant collimation and dose decreases in regions outside the plaque radius relative to the dose for the same configurations of seeds in water, as demonstrated in Fig. 5 for a 16 mm plaque fully loaded with ^{125}I seeds. Near the plaque, e.g., at $z=0.25$ cm, the dose decreases substantially relative to water at the trans-

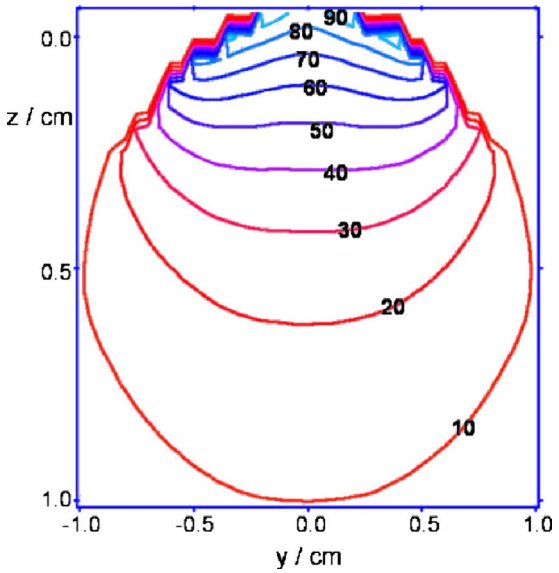

FIG. 6. Isodose contours in the y, z plane (x=0) for a 16 mm Modulay/Silastic plaque with ^{125}I seeds. The dose is scored in (0.05 cm)^3 voxels and is set to zero in voxels intersecting the plaque, resulting in the ridges seen in the upper part of the figure.

verse position y=0.8 cm, corresponding to the plaque's radius. As the distance (z) from the plaque increases, this dose decrease relative to water occurs at larger transverse positions. This is also illustrated in Fig. 6, which displays the isodose contours in the y, z plane (x=0) for the 16 mm Modulay/Silastic plaque with ^{125}I seeds. The collimation and off-axis dose decreases relative to water are similar for ^{103}Pd seeds. For smaller (larger) plaque sizes, the dose decrease relative to water becomes more significant at smaller (larger) values of the transverse coordinate.

Full simulations, including interseed effects, for each COMS plaque size (Modulay/Silastic combination) are performed for the plaques in water. The three-dimensional dose distributions for (0.05 cm)^3 voxels are posted at http://www.physics.carleton.ca/clrp/eye_plaque. Multiseed central

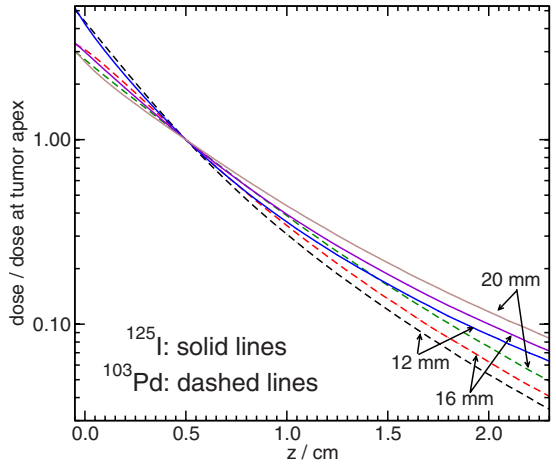

FIG. 7. Comparison of plaque central axis depth-dose curves for ^{125}I and ^{103}Pd for various plaque sizes (Modulay plaque, Silastic insert).

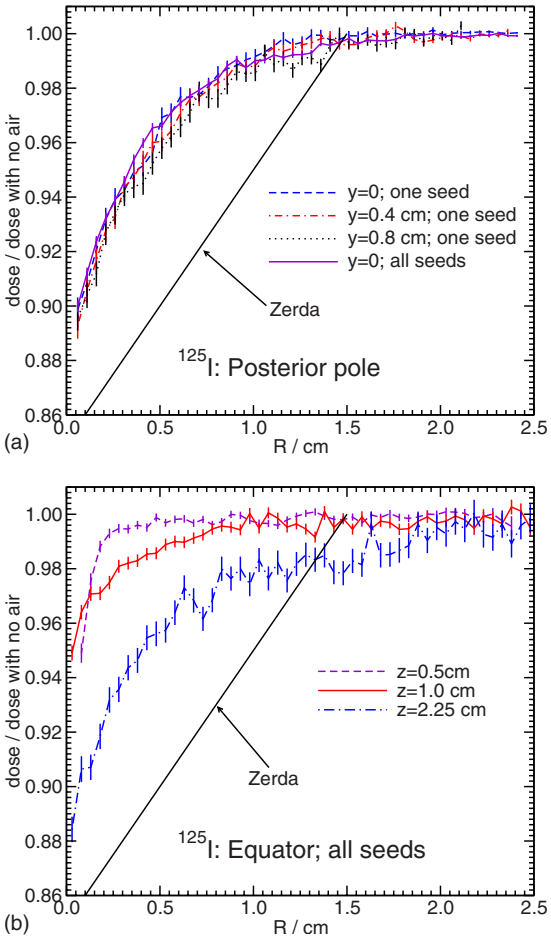

FIG. 8. The effect of an air interface for ^{125}I: The ratio of the doses with an air interface to the doses with no air vs the distance from the air interface, R, for a 20 mm Modulay/Silastic plaque. In (a), the plaque is on the posterior-pole and results are for x=0 and various transverse positions y. In (b), the plaque is on the equator and the results are given for different depths z. The label "all seeds" indicates that the results are for a fully loaded plaque (24 seeds); otherwise, there is one seed in the plaque's central slot. The line marked "Zerda" is the best-fit line of de la Zerda *et al.* (Ref. 15).

axis depth-dose curves for the 12, 16, and 20 mm plaque sizes and both seed types are presented in Fig. 7, where the dose is quoted relative to the dose at the tumor apex or prescription point (z=0.5 cm). In general, the dose in the tumor (z<0.5 cm) is higher for ^{103}Pd seeds than for ^{125}I for a given plaque size. Beyond the apex, the dose with ^{103}Pd seeds drops off more rapidly.

III.D. Towards a full human eye model: The air interface and other effects

The introduction of an air interface at the edge of the eye (see Fig. 1) results in a dose decrease (relative to water) in this region, due to the reduction in backscattered radiation. This reduction depends on the plaque's position and size as well as the radionuclide type and number of seeds. Generally, the effect of the air interface is larger for ^{125}I than it is for ^{103}Pd as there is less scatter for the lower-energy ^{103}Pd photons. Figures 8 and 9 display the dose reduction due to the air interface for ^{125}I and ^{103}Pd seeds, respectively, for

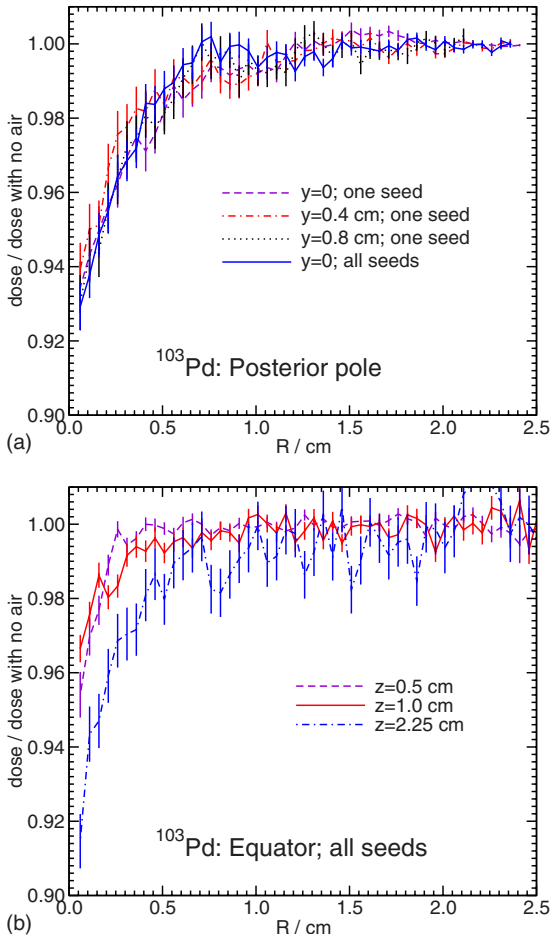

FIG. 9. The effect of an air interface for ^{103}Pd: The ratio of the doses with an air interface to the doses with no air vs the distance to the air interface, R, for a 20 mm Modulay/Silastic plaque. The plaque positions and labeling are as in Fig. 8.

plaques centered (a) on the posterior pole and (b) on the equator temporal to the eyeball. In each of these figures, the ratio of the dose with the air interface to that without the air interface is shown for a 20 mm plaque as a function of the (transverse) distance to the air interface R. For the plaque centered on the posterior pole, the central axis coordinate z is related to this distance via $z=2.36\ \text{cm}-R$, while for the plaque centered on the equator, the coordinate x which spans one direction transverse to the central axis is related to R via $x=1.23\ \text{cm}-R$.

Consider first the case (a) in which the plaque is centered on the optic axis in the eye posterior. Figures 8(a) and 9(a) display dose ratios for a single seed in the central slot on the plaque's central axis $(x,y=0)$ and also off-axis $(x=0,\ y=0.4,\ 0.8\ \text{cm})$. The analogous ratios for a fully loaded plaque are very close to those for the single seed, and so only the central axis results are plotted in these figures for the fully loaded plaque. Hence, the dose decrease is not very sensitive to the number of seeds in the plaque. The dose reduction is most important in the immediate vicinity of the air interface and decreases as R increases. Near the interface, the dose decrease is of the order of 10% for ^{125}I and 7% for ^{103}Pd. At $R=0.5$ cm, the dose reduction is already of the order of 4% for ^{125}I and 2%–3% for ^{103}Pd. Near $R\simeq 1.5$ cm, the effect of the air interface is negligible. The dose in the region where the effect of the air interface is important is already small: Fig. 7 reveals that the dose at $R=0.5$ cm, which is near the center of the lens, is only 14% of the prescription dose for ^{125}I and 10% for ^{103}Pd. The dose ratio (air relative to no air) is roughly the same for other plaque sizes.

The straight line in Fig. 8(a) represents the best-fit line of de la Zerda *et al.*,[15] based on their TLD measurements for the same single ^{125}I seed configuration. This linear function is used in Plaque Simulator to account for the effect of the air interface and clearly overestimates the dose decrease. In principle, the discrepancy between the results in Fig. 8(a) and those of de la Zerda *et al.* might be partially attributable to the difference in size of the region in which dose is scored in our MC simulations and dose is measured in the TLD experiments. However, scoring in $(0.1\ \text{cm})^3$ voxels yields results in agreement with those for the smaller voxel size, presented in Fig. 8(a). Examining Fig. 8(a) carefully, one finds that the dose decrease is slightly more important at off-axis points than on the central axis. This was not observed by de la Zerda *et al.* Their line is the best fit to the average of data on and off the central axis and seems to be quite noisy: For example, at $x=0$, $y=1.0$ cm, and $R\simeq 1.2$ cm, their dose with air is 7% higher than when no air is present, compared to the less than 1% decrease shown in Fig. 8(a).

Figures 8(b) and 9(b) show the dose ratio for a fully loaded 20 mm plaque centered on the equator. The dose drop-off depends on the distance from the plaque, z. The distance from the air interface at which the effects of the air become significant is also dependent on the distance from the plaque. Near the plaque, e.g., $z=0.5$ cm, the dose decrease is only significant within a couple of millimeters of the air interface; however, further away, e.g., $z=2.25$ cm, the dose decrease is non-negligible at $R\simeq 1$ cm. However, the dose in the region where the dose decrease is more important (i.e., far from the plaque) is also the region where the dose is very small: Fig. 7 shows that the dose is less than 12% of the prescription dose for ^{125}I and 7% for ^{103}Pd. In the vicinity of the lens, the dose decrease due to the air is less than 2%. The linear function of de la Zerda *et al.*, used in Plaque Simulator to account for the air interface for all plaque configurations, is also shown in Fig. 8(b) and again, clearly overestimates the dose decrease.

A 1 mm thick lead sheet 5 mm away from the eye-air interface (representing a lead eye patch) causes a smaller dose decrease than if only air is present: The excitation of the L-shell in the lead ($\sim$16 keV) results in the emission of fluorescence photons which scatter back into the eye. For a 20 mm plaque containing one ^{125}I seed centered on the optic axis in the eye's posterior, the dose decrease at the edge of the eye is less than 5%, compared to 10% when only air is present.

The presence of bony material about the eye region results in a dose decrease due to enhanced photoelectric absorption and reduced scatter, as illustrated in Fig. 10 for a

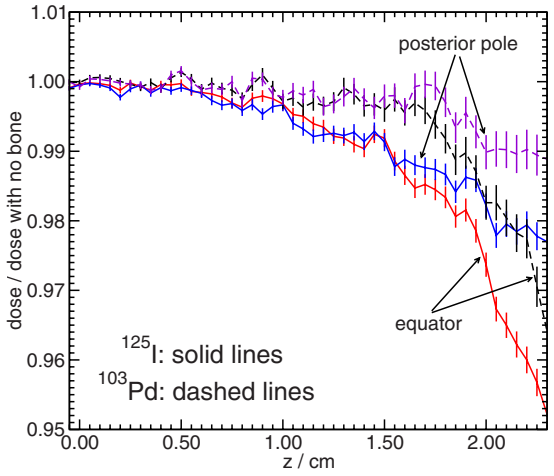

FIG. 10. The effect of a cylinder (of diameter 3.01 cm) of bone about the eye. The ratio of doses with bone to the doses with no bone vs the position z along the plaque's central axis for a 20 mm Modulay/Silastic plaque fully loaded with either ^{125}I or ^{103}Pd seeds. The plaque is centered on the posterior pole or on the equator temporal to the eyeball.

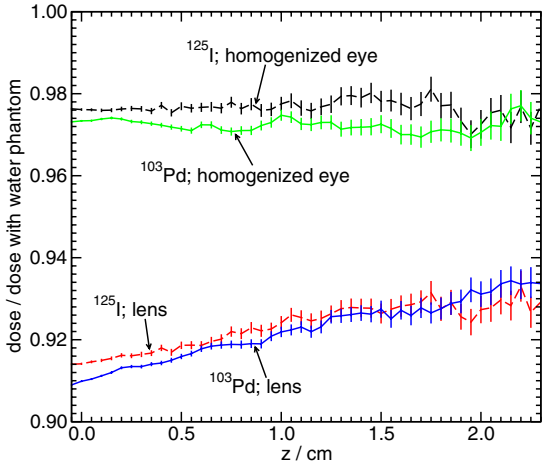

FIG. 11. Dose deposited in a phantom made of homogenized eye or lens material relative to dose deposited in a water phantom for one ^{125}I or ^{103}Pd seed in the central slot of a 20 mm Modulay/Silastic plaque vs position along the plaque's central axis.

fully loaded 20 mm (Modulay/Silastic) plaque on the posterior pole and on the equator temporal to the eyeball. For either plaque position, the effect of the bone is more significant for ^{125}I seeds than for ^{103}Pd. Once again, this is because Compton scatter accounts for a greater proportion of ^{125}I photon interactions in water and the main effect of the bone is to reduce this scatter, resulting in a larger dose decrease for ^{125}I than for ^{103}Pd. The dose decrease at the opposite side of the eyeball to the plaque is near 3.5% for ^{103}Pd and 5% for ^{125}I for a plaque on the equator temporal to the eyeball. This decrease is less significant (1% for ^{103}Pd and 2% for ^{125}I) for the plaque centered on the posterior pole. Though not shown, decreasing the diameter of the bone cylinder results in larger dose decreases: For the plaque on the posterior pole, the dose decrease at the opposite side of the eye to the plaque is 2% for ^{103}Pd and 4% for ^{125}I.

For all the simulations reported to date, dose is scored in water, in accord with usual brachytherapy calculation protocols. However, the eye is made up of a variety of materials with elemental compositions and densities different from water. Replacing the water with these eye materials results in dose differences, as illustrated in Fig. 11, because the mass energy absorption coefficients for these materials differ from those for water: μ_{en}/ρ is lower for both the homogenized eye (~2–3% for 21, 28 keV photons) and lens (~9% for 21, 28 keV photons) materials. As dose is proportional to the fluence times μ_{en}/ρ, near the seed, where the fluence is nearly the same for each configuration, the dose differs by the ratio of μ_{en}/ρ values and hence it is lower for both the homogenized eye and lens materials relative to water because of the differences in energy absorption coefficients. In the homogenized eye material, the dose relative to water stays nearly constant going across the eye because the increased density is almost exactly counteracted by the difference in the attenuation coefficient. In the lens material, the photon fluence increases relative to water because the difference in attenuation coefficients is not quite balanced by the density difference; a gradient in the ratio of the dose deposited in the material to the dose deposited in water across the eye results.

III.E. Dose comparison at points of interest

This section brings together many of the effects discussed above by comparing the dose at points of interest for different plaque materials, configurations, and the two seed types. Tables III and IV provide the dose at points of interest (see Fig. 1) for a 16 mm plaque fully loaded with ^{125}I or ^{103}Pd seeds on the equator temporal to the eyeball (Table III) and between the equator and posterior pole (Table IV). The air kerma strength per seed (S_K) required to obtain a dose of 85 Gy at the prescription point for the seeds in water with no interseed effects for a treatment time of 100 h for ^{125}I and 168 h for ^{103}Pd is given. For this air kerma strength, the doses for the Modulay/Silastic combination are given, as are the doses when the air interface is present. The presence of the Modulay and Silastic causes a consistent decrease in the dose to the normal ocular structures. As noted above, the effect of the air interface at these points of interest is generally small. For example, for the plaque positioned between the equator and posterior pole, the dose decrease due to the air is of order 3% for the lens and 5% at the opposite side for the ^{125}I seeds, and even smaller for ^{103}Pd. If the plaque centered on the equator temporal to the eyeball is moved to the superior position with a rotation through 90° about the optic axis, only the dose at the optic nerve will change because of the symmetries of the configuration. This is also true if the plaque position is rotated a further 90° about the optic axis so that it is centered on the equator nasal to the eyeball. Table III also provides the dose at the optic nerve for these configurations.

The doses to the points of interest in Tables III and IV are also presented as percentages of the prescription dose (D_p), which facilitates the comparison of the doses for the two

TABLE III. Comparison of the dose at points of interest for a 16 mm (fully loaded with 13 seeds) plaque on the equator temporal to the eyeball. The columns labeled "Water" indicate the dose for the seeds in water with no plaque present and no interseed effects, while the label "MS" indicates the Modulay/Silastic combination. The results when the air interface is present are also included as percentages of the prescription dose, D_p. Doses to the optic disk are included for the plaque on the equator nasal to the eyeball ("nasal") and centered on the equator above or below the eyeball ("above or below"). The air kerma strength per seed S_K required to obtain a prescription dose of 85 Gy at the tumor apex in 100 h for model 6711 ^{125}I seeds and 168 h for model 200 ^{103}Pd seeds ("Water" configuration) is indicated where 1 U=1 μGy m^2 h^{-1}. The statistical uncertainties are less than 0.34% for ^{125}I and 0.50% for ^{103}Pd.

	^{125}I				^{103}Pd			
			MS, air				MS, air	
Location	Water Gy	MS Gy	Gy	% of D_p	Water Gy	MS Gy	Gy	% of D_p
Center of eye	27.92	23.79	23.68	32	22.75	18.23	18.19	27
Macula	16.45	12.82	12.80	17	11.40	8.089	8.094	12
Optic disk (temporal)	11.35	8.989	8.947	12	7.193	5.355	5.297	8
Center of lens	21.75	17.85	17.53	24	16.34	12.50	12.41	18
Sclera	262.1	222.9	222.7	299	287.9	210.7	210.6	307
Apex	(85.00)	74.43	74.40	(100)	(85.00)	68.53	68.54	(100)
Opposite side	6.830	5.550	5.453	7	3.771	2.930	2.956	4
Optic disk (nasal)	27.78	21.02	20.97	28	21.65	14.13	14.18	21
Optic disk (above or below)	16.49	12.81	12.78	17	11.38	8.104	8.088	12
S_K	4.76 U/seed			—	4.04 U/seed			—

seed types. Apart from the scleral dose, which is less than 3% higher for ^{103}Pd than for ^{125}I seeds, the dose at all points of interest is lower with ^{103}Pd seeds. The fact that the dose with ^{103}Pd seeds is higher within the tumor was noted and seen in Fig. 7 above. The results presented here for the 16 mm plaque size are representative of the results for other plaque sizes.

Table V compares the dose rates at points of interest for a 12 mm plaque between the posterior pole and equator (as in Fig. 1) and a 20 mm plaque centered on the equator temporal to the eyeball from the BrachyDose simulations to those of Astrahan,[17] obtained with Plaque Simulator. The most notable discrepancy is for the 20 mm plaque configuration, where Plaque Simulator overestimates the dose by 10% at the optic disk and 11% at the macula. Agreement with the 12 mm plaque results is surprisingly good considering the observations made above regarding the factors used in Plaque Simulator to account for the Modulay/Silastic combination and the air interface.

IV. CONCLUSION

In this study, the BrachyDose code was used to investigate various aspects of eye plaque dosimetry: the separate and combined effects of the plaque backing and insert, interseed attenuation, dose decreases due to an air interface or orbital bones, and scoring in various eye materials (rather than water). The presence of the plaque backing alone (water insert) results in a dose enhancement near the plaque due to fluorescence photons, and a decrease at larger distances due to the decrease in scatter, relative to water. The results for the Modulay and pure gold backings differ, indicating sensitivity

TABLE IV. Comparison of dose at points of interest for a 16 mm plaque midway between the posterior pole and equator temporal to the eyeball, as shown in Fig. 1. The labeling and uncertainties are as in Table III, and again the treatment time is taken to be 100 (168) h for ^{125}I (^{103}Pd).

	^{125}I				^{103}Pd			
			MS, air				MS, air	
Location	Water Gy	MS Gy	Gy	% of D_p	Water Gy	MS Gy	Gy	% of D_p
Center of eye	27.92	23.79	23.71	32	22.75	18.23	18.22	27
Macula	74.32	58.99	58.97	79	70.04	47.32	47.31	69
Optic disk	31.32	23.16	23.06	31	25.09	15.97	15.99	23
Center of lens	12.35	10.20	9.892	13	8.147	6.381	6.301	9
Sclera	262.1	222.9	222.6	299	287.9	210.7	210.9	308
Apex	(85.00)	74.43	74.44	(100)	(85.00)	68.53	68.56	(100)
Opposite side	6.830	5.550	5.293	7	3.771	2.930	2.886	4
S_K	4.76 U/seed			—	4.04 U/seed			—

TABLE V. Comparison of the dose rates (in cGy/h) at points of interest obtained using BrachyDose ($\dot{D}_{BD}$) to those of Astrahan (Ref. 17) using Plaque Simulator ($\dot{D}_{PS}$). The results are for a 12 mm plaque midway between the posterior pole and equator temporal to the eyeball and a 20 mm plaque centered on the equator temporal to the eyeball. Both plaques are filled with model 6711 ^{125}I seeds with S_K=1.27 U/seed. The statistical (1σ) uncertainties on the BrachyDose results are less than 0.34%.

	12 mm			20 mm		
Location	$\dot{D}_{PS}$	$\dot{D}_{BD}$	$\dot{D}_{PS}/\dot{D}_{BD}$	$\dot{D}_{PS}$	$\dot{D}_{BD}$	$\dot{D}_{PS}/\dot{D}_{BD}$
Macula	5.851	6.086	0.96	7.796	6.986	1.12
Optic disk	3.072	3.071	1.00	5.278	4.795	1.10
Center of lens	1.599	1.610	0.99	9.268	9.422	0.98
Sclera	58.00	58.93	0.98	88.23	88.06	1.00
Opposite side	0.855	0.8673	0.99	2.981	2.874	1.04

to the backing's composition. The Silastic insert causes substantial attenuation. The Silastic/Modulay combination results in a dose decrease relative to water of roughly 14% and 20% for ^{125}I and ^{103}Pd, respectively, at $z \simeq 1$ cm on the plaque's central axis. The decrease depends on the plaque size and number of seeds. Interseed attenuation is a small, less than 2%, effect for the region of interest in eye plaque dosimetry with COMS plaques. The presence of an air interface results in a dose decrease in the vicinity of the interface due to the reduction in backscattered radiation; however, generally the dose to the tumor is unchanged. Dose reductions result from the introduction of bone in the eye's vicinity. Finally, scoring in various eye materials results in dose differences (and sometimes gradients across the eye) relative to the dose deposited in water.

Doses at points of interest within the eye were compared for different plaque configurations. The presence of the Modulay and Silastic results in consistent dose decreases at these points of interest compared to the dose for the same configurations of seeds in water. Apart from the sclera, ^{103}Pd seeds generally offer lower doses to the critical normal structures than do ^{125}I seeds.

On a single 3.0 GHz Woodcrest core, BrachyDose can achieve 2% statistical uncertainty on the dose to the tumor apex in 3 min for $(0.05\ \text{cm})^3$ voxels; for $(0.1\ \text{cm})^3$ voxels, which should be sufficient for clinical applications, it takes about 30 s. Requiring 2% statistical uncertainty on the dose at the point where the dose is half that at the tumor apex takes twice as long: Less than 6 min for the $(0.05\ \text{cm})^3$ voxels and 1 min for the $(0.1\ \text{cm})^3$ voxels. These times are sufficiently fast for routine clinical treatment planning.

BrachyDose is a powerful tool to explore eye plaque dosimetry which can be adapted to different plaque designs and seed models. Dosimetry for other plaque designs or different seed models would be a straightforward extension of the work presented here. Investigating dose distributions for partially filled plaques or for plaques with cutouts is also possible. As BrachyDose is based on the EGSnrc system, electron transport may be modeled which would allow the investigation of beta ray sources such as ^{106}Ru for eye plaque brachytherapy. For accurate dosimetry, a detailed human eye model should be integrated into these simulations. This could lead to significant changes in the dose distributions, as shown in Fig. 11.

ACKNOWLEDGMENTS

The authors acknowledge support from the Natural Sciences and Engineering Research Council of Canada (NSERC), the Canada Research Chairs program (DWOR), the Canada Foundation for Innovation (CFI), the Ontario Innovation Trust (OIT), the office of the Vice-President of Research at Carleton University, and the L'Oréal Canada/UNESCO Research Excellence Fellowship program (RMT). We also wish to thank the members of the Carleton Laboratory for Radiotherapy Physics and the referees for their comments on this article.

[a]Electronic mail: rthomson@physics.carleton.ca

[1]J. Earle, R. W. Kline, and D. M. Robertson, "Selection of iodine-125 for the Collaborative Ocular Melanoma Study," Arch. Ophthalmol. (Chicago) **105**, 763–764 (1987).
[2]Collaborative Ocular Melanoma Study Group, "The COMS randomized trial of iodine 125 brachytherapy for choroidal melanoma. III. Initial Mortality findings. COMS Report No. 18," Arch. Ophthalmol. (Chicago) **105**, 969–982 (2001).
[3]Collaborative Ocular Melanoma Study Group, "The COMS randomized trial of iodine 125 brachytherapy for choroidal melanoma. V. Twelve-year mortality rates and prognostic factors: COMS Report No. 28," Arch. Ophthalmol. (Chicago) **124**, 1684–1693 (2006).
[4]R. W. Kline and P. D. Yeakel, "Ocular melanoma, I-125 plaques," Med. Phys. **14**, 475 (Abs) (1987).
[5]Collaborative Ocular Melanoma Study Group, *COMS Manual of Procedures*, Ch. 12: Radiation therapy, COMS manual of procedures PB95-179693 (National Technical Information Service, Springfield, VA, 1995).
[6]R. Nath, L. L. Anderson, G. Luxton, K. A. Weaver, J. F. Williamson, and A. S. Meigooni, "Dosimetry of interstitial brachytherapy sources: Recommendations of the AAPM Radiation Therapy Committee Task Group No. 43," Med. Phys. **22**, 209–234 (1995).
[7]K. A. Weaver, "The dosimetry of ^{125}I seed eye plaques," Med. Phys. **13**, 1032–1040 (1986).
[8]G. Luxton, M. A. Astrahan, and Z. Petrovich, "Backscatter measurements from a single seed of ^{125}I for ophthalmic plaque dosimetry," Med. Phys. **15**, 397–400 (1988).
[9]A. Wu, E. S. Sternick, and D. J. Muise, "Effect of gold shielding on the dosimetry of an I-125 seed at close range," Med. Phys. **15**, 627–628 (1988).
[10]J. Cygler, J. Szanto, M. Soubra, and D. W. O. Rogers, "Effects of gold and silver backings on the dose rate around an ^{125}I seed," Med. Phys. **17**, 172–178 (1990).
[11]A. Wu and F. Krasin, "Film dosimetry analyses on the effect of gold

shielding for Iodine-125 eye plaque therapy for choroidal melanoma," Med. Phys. **17**, 843–846 (1990).
[12]J. A. Meli and K. A. Motakabbir, "The effect of lead, gold, and silver backings on dose near ^{125}I seeds," Med. Phys. **20**, 1251–1256 (1993).
[13]M. Astrahan, G. Luxton, G. Jozsef, T. D. Kampp, P. Liggett, and M. D. Sapozink, "An interactive treatment planning system for ophthalmic plaque radiotherapy," Int. J. Radiat. Oncol., Biol., Phys. **18**, 679–687 (1990).
[14]S. Chiu-Tsao, L. L. Anderson, K. O'Brien, L. Stabile, and J. C. Liu, "Dosimetry for ^{125}I seed (model 6711) in eye plaques," Med. Phys. **20**, 383–389 (1993).
[15]A. de la Zerda, S. Chiu-Tsao, J. Lin, L. L. Boulay, I. Kanna, and H. Tsao, "^{125}I plaque dose distribution including penumbra characteristics," Med. Phys. **23**, 407–418 (1996).
[16]A. L. Krintz, W. F. Hanson, G. S. Ibbott, and D. S. Followill, "A reanalysis of the collaborative ocular melanoma study medium tumor trial eye plaque dosimetry," Int. J. Radiat. Oncol., Biol., Phys. **56**, 889–898 (2003).
[17]M. A. Astrahan, "Improved treatment planning for COMS eye plaques," Int. J. Radiat. Oncol., Biol., Phys. **61**, 1227–1242 (2005).
[18]P. T. Finger, D. M. Moshfeghi, and T. K. Ho, Palladium-103 ophthalmic plaque radiotherapy, Arch. Ophthalmol. (Chicago) **109**, 1610–1613 (1991).
[19]P. T. Finger, D. Lu, A. Buffa, D. S. DeBlasio, and J. L. Bosworth, "Palladium-103 versus Iodine-125 for ophthalmic plaque radiotherapy," Int. J. Radiat. Oncol., Biol., Phys. **27**, 849–854 (1993).
[20]P. T. Finger, A. Berson, and A. Szechter, "Palladium-103 plaque radiotherapy for choroidal melanoma," Ophthalmology **106**, 606–613 (1999).
[21]P. T. Finger, A. Berson, N. Tracy, and A. Szechter, "Palladium-103 plaque radiotherapy for choroidal melanoma: An 11 year study," Int. J. Radiat. Oncol., Biol., Phys. **54**, 1438–1445 (2002).
[22]M. J. Rivard, B. M. Coursey, L. A. DeWerd, M. S. Huq, G. S. Ibbott, M. G. Mitch, R. Nath, and J. F. Williamson, "Update of AAPM Task Group No. 43 Report: A revised AAPM protocol for brachytherapy dose calculations," Med. Phys. **31**, 633–674 (2004).
[23]S. Chiu-Tsao, L. Boulay, I. Kanna, A. de la Zerda, and J. H. Kim, "Dose distribution in the eye for ^{103}Pd seed in COMS eye plaque," Med. Phys. **22**, 923 (Abs.) (1995).
[24]W. Alberti, "Acute and late side effects of radiotherapy for ocular disease: An overview," in *Radiotherapy of Ocular Diseases*, edited by T. Wiegel, N. Bornfeld, M. H. Foerster, and W. Hinkelbein (S. Karger AG, Basel, 1997), pp. 281–286.
[25]ICRU, Dosimetry of Beta-Rays and Low-Energy Photons for Brachytherapy with Sealed Sources, ICRU Report 72, ICRU, Washington D. C., 2004.
[26]S. Nag, J. M. Quivey, J. D. Earle, D. Followill, J. Fontanesi, and P. T. Finger, "The American brachytherapy society recommendations for brachytherapy of uveal melanomas," Int. J. Radiat. Oncol., Biol., Phys. **56**, 544–555 (2003).
[27]C. S. Melhus and M. J. Rivard, "COMS eye plaque brachytherapy dosimetry simulations for ^{103}Pd, ^{125}I, and ^{131}Cs," Med. Phys. **35**, 3364–3371 (2008).
[28]G. Yegin and D. W. O. Rogers, "A fast Monte Carlo code for multi-seed brachytherapy treatments including interseed effects," Med. Phys. **31**, 1771 (Abs.) (2004).
[29]G. Yegin, R. E. P. Taylor, and D. W. O. Rogers, BrachyDose: "A new fast Monte Carlo code for brachytherapy calculations," Med. Phys. **33**, 2075–2075 (Abs.) (2006).
[30]I. Kawrakow and D. W. O. Rogers, "The EGSnrc code system: Monte Carlo simulation of electron and photon transport," Technical Report PIRS–701, National Research Council of Canada, Ottawa, Canada, 2000.
[31]I. Kawrakow, "Accurate condensed history Monte Carlo simulation of electron transport. I. EGSnrc, the new EGS4 version," Med. Phys. **27**, 485–498 (2000).
[32]H. E. Johns and J. R. Cunningham, *The Physics of Radiology*, 4th ed. (Charles C. Thomas, Springfield, IL, 1983).
[33]M. J. Berger and J. H. Hubbell, "XCOM: Photon cross sections on a personal computer," Report NBSIR87–3597, National Institute of Standards Technology (NIST), Gaithersburg, MD 20899, 1987.
[34]G. Yegin, "A new approach to geometry modelling of Monte Carlo particle transport: an application to EGS," Nucl. Instrum. Methods Phys. Res. B **211**, 331–338 (2003).
[35]R. E. P. Taylor, G. Yegin, and D. W. O. Rogers, "Benchmarking BrachyDose: Voxel-based EGSnrc Monte Carlo calculations of TG–43 dosimetry parameters," Med. Phys. **34**, 445–457 (2007).
[36]R. E. P. Taylor and D. W. O. Rogers, "An EGSnrc Monte Carlo-calculated database of TG-43 parameters," Med. Phys. **35**, 4228–4241 (2008).
[37]R. E. P. Taylor and D. W. O. Rogers, The Carleton Laboratory for Radiotherapy Physics TG-43 Parameter Database, http://www.physics.carleton.ca/clrp/seed_database.
[38]S. Chiu-Tsao, "Episcleral eye plaques for treatment of intraocular malignancies and benign diseases," in *Brachytherapy Physics*, edited by B. R. Thomadsen, M. J. Rivard, and W. M. Butler (Medical Physics Publishing, Madison, WI, 2005), pp. 673–705.
[39]ICRU, Photon, Electron, Photon and Neutron Interaction Data for Body Tissues, ICRU Report 46, ICRU, Washington D.C., 1992.
[40]S. Chiu-Tsao, K. O'Brien, R. Sanna, H. Tsao, C. Vialotti, Y. Chang, M. Rotman, and S. Packer, "Monte Carlo dosimetry for ^{125}I and ^{60}Co in eye plaque therapy," Med. Phys. **13**, 678–682 (1986).
[41]A. G. Kepka, P. M. Johnson, and R. W. Kline, "The generalized geometry of eye plaque therapy," Med. Phys. **15**, 375–379 (1988).
[42]B. R. B. Walters, I. Kawrakow, and D. W. O. Rogers, "History by history statistical estimators in the BEAM code system," Med. Phys. **29**, 2745–2752 (2002).
[43]O. Chibani, J. F. Williamson, and D. Todor, "Dosimetric effects of seed anisotropy and interseed attenuation for ^{103}Pd and ^{125}I prostate implants," Med. Phys. **32**, 2557–2566 (2005).